

PHASE TRANSITIONS IN MESOSCOPIC SUPERCONDUCTING FILMS

V. V. Kabanov

J. Stefan Institute, Jamova 39, 1000 Ljubljana, Slovenia
viktor.kabanov@ijs.si

T. Mertelj

Faculty of Mathematics and Physics, Jadranska 19, 1000 Ljubljana, Slovenia
and
J. Stefan Institute, Jamova 39, 1000 Ljubljana, Slovenia
tomaz.mertelj@ijs.si

Abstract We solve the Ginzburg-Landau equation (GLE) for the mesoscopic superconducting thin film of the square shape in the magnetic field for the wide range of the Ginzburg-Landau parameter $0.05 < \kappa_{eff} < \infty$. We found that the phase with the antivortex exists in the broad range of parameters. When the coherence length decreases the topological phase transition to the phase with the same total vorticity and a reduced symmetry takes place. The giant vortex with the vorticity $m = 3$ is found to be unstable for any field, ξ/a and $\kappa_{eff} \geq 0.1$. Reduction of κ_{eff} does not make the phase with antivortex more stable contrary to the case of the cylindrical sample of the type I superconductor.

Introduction

Advances in nanotechnology and constantly shrinking semiconductor devices have motivated researches to study properties of mesoscopic superconducting samples. One line of research in this field has focused on the problem of the phase transitions in the mesoscopic superconducting sample under the influence of the external magnetic field. [1] We will focus on the case when the size of the sample $a \sim \xi, \lambda$, with ξ and λ being the superconducting coherence length and the London penetration depth respectively. In that case there are only a few vortices in the sample. The standard Abrikosov approach [2] must be modified because of the strong influence of sample boundaries. Thermodynamics of the system is determined by the short-range repulsion of vortices and interaction of vortices with boundaries.

Recently it was shown that the influence of boundaries can lead to stabilization of the vortex-antivortex molecules in mesoscopic samples.[1] Analysis of the linearized Ginzburg-Landau equation (GLE) has shown that such molecules appear at particular values of the external magnetic field depending on the sample shape and size[3]. The solution of the GLE in the limit of the extreme type-II superconductor shows that such molecules have a very shallow minimum in the free energy[4, 5] and are very sensitive to the change of the sample shape[6].

In a square mesoscopic thin film with the total vorticity $m = 3$ the symmetric solution with four vortices and one antivortex is the solution of the linearized GLE with the lowest free energy[1]. According to ref. [4], away from the H_{c2} line the giant vortex with vorticity $m = 3$ is stable and has the lowest free energy. This implies that a topological phase transition *without change* of the vorticity and *without a reduction* of the symmetry should take place with the change of the external field or/and the coherence length away from the critical-field line.

Here we report the results of the extensive studies of different kinds of phase transitions for the thin film of the square shape. We focused to the region $4 < a/\xi < 8$ and $\kappa_{eff} > 0.05$ (see also[7]). Here $\kappa_{eff} = \lambda^2/d\xi$ where d is the film thickness. We found that the antivortex phase with $m = 3$ is stable in a broad range of parameters. The region of stability of the phase does not depend strongly on the value of the parameter κ_{eff} . The energy gain due to the antivortex formation is much smaller than the energy difference between two phases with different vorticities. The giant vortex with $m = 3$ is unstable for any field, ξ/a and $\kappa_{eff} \geq 0.1$. Phase transition to the phase with three separated vortices takes place when ξ/a is driven away from the critical field line. The reduction of κ_{eff} does not stabilize the antivortex phase for the thin film sample in the contrast to the case of the cylindrical sample ref.[8].

1. Formalism and Solution

GLE for the normalized complex order parameter ψ has the following form: [4]

$$\xi^2 \left(i\nabla + \frac{2\pi\mathbf{A}}{\Phi_0} \right)^2 \psi - \psi + \psi|\psi|^2 = 0 \quad (1)$$

here Φ_0 is the flux quantum, \mathbf{A} is the vector potential and $\mathbf{H} = \nabla \times \mathbf{A}$ the magnetic field. We split the vector potential into the external part due to external currents, \mathbf{A}_{ext} , and the internal part due to the response of the superconducting film, \mathbf{A}_{int} . The second GLE equation for the total vector potential reads:

$$\nabla \times \nabla \times \mathbf{A} = -i \frac{\Phi_0}{4\pi\lambda^2} (\psi^* \nabla \psi - \psi \nabla \psi^*) - \frac{|\psi|^2 \mathbf{A}}{\lambda^2}. \quad (2)$$

In addition to Eq.(1) we assume the boundary condition for the superconductor insulator junction on the sample edges:

$$(i\nabla + \frac{2\pi\mathbf{A}}{\Phi_0}) \cdot \mathbf{n}\psi = 0, \quad (3)$$

where \mathbf{n} is the vector normal to the surface of the sample.

As it was described in ref.[4] we introduce $N \times N$ discrete points on the square and rewrite Eq. (1) in the form of the nonlinear discrete Schrödinger equation:

$$\sum_{\mathbf{l}} t_{\mathbf{l},\mathbf{i}}\psi_{\mathbf{l}} - \epsilon(\mathbf{i})t_{\mathbf{i},\mathbf{l}}\psi_{\mathbf{i}} - \psi_{\mathbf{i}} + \psi_{\mathbf{i}}|\psi_{\mathbf{i}}|^2 = 0, \quad (4)$$

where the summation index $\mathbf{l} = (\pm 1, 0), (0, \pm 1)$ points toward the nearest neighbors and $t_{\mathbf{l},\mathbf{i}} = (\xi N/a)^2 \exp(i\phi_{\mathbf{l},\mathbf{i}})$ and $\phi_{\mathbf{l},\mathbf{i}} = -\frac{2\pi}{\Phi_0} \int_{\mathbf{r}_i}^{\mathbf{r}_{i+\mathbf{l}}} \mathbf{A}(\mathbf{r})d\mathbf{r}$. The boundary conditions are included in the discrete nonlinear Schrödinger equation as in ref.[4] where $\psi_{\mathbf{i}} = 0$ if \mathbf{i} is outside of the sample and $\epsilon(\mathbf{i}) = 4 - \delta_{i_x,1} - \delta_{i_x,N} - \delta_{i_y,1} - \delta_{i_y,N}$ where $\mathbf{i} = (i_x = 1, \dots, N, i_y = 1, \dots, N)$.

After discretization of Eq. (2) we obtain the exact expression for the internal part of the vector potential[7]:

$$A_{int,\mathbf{i}}^v = \sum_{\mathbf{n}} K(\mathbf{i} - \mathbf{n})J_{\mathbf{n}}^v, \quad (5)$$

where

$$J_{\mathbf{i}}^v = \frac{\Phi_0 a}{4\pi\lambda_{eff}N} \Im(\exp(-i\phi_{\mathbf{i}+\mathbf{l}_v,\mathbf{i}})\psi_{\mathbf{i}}^*\psi_{\mathbf{i}+\mathbf{l}_v} - \exp(-i\phi_{\mathbf{i}-\mathbf{l}_v,\mathbf{i}})\psi_{\mathbf{i}}^*\psi_{\mathbf{i}-\mathbf{l}_v}) \quad (6)$$

with $v \in \{x, y\}$ and $\mathbf{l}_x = (1, 0)$, $\mathbf{l}_y = (0, 1)$ and

$$K(\mathbf{n}) = \frac{N}{2\pi^2 a} \int_0^\pi dx dy \frac{\cos(n_x x) \cos(n_y y)}{\sqrt{4 - 2\cos(x) - 2\cos(y)}}. \quad (7)$$

Here we should point out that Eq.(5) contains 2D integration only[7]. All dependence on the thickness of the sample appears through the parameter $\lambda_{eff} = \lambda^2/d$ (d is the thickness of the sample)[9]. This is important difference from the case of the cylindrical sample considered in the Ref.[8] where the function $K(\mathbf{n})$ is essentially different.

The numerical self consistent solution of the problem is obtained by iterating the solution of the nonlinear equation for the order parameter Eq.(4) and calculations of the current and the vector potential Eqs.(5,6). We used two ways of solving Eq.(4). The first is similar to that reported in ref.[4] and corresponds to the iterative solution of the linearized Eq.(4). The second relies on the fact that Eq.(4) represents the Euler equation for the free-energy functional

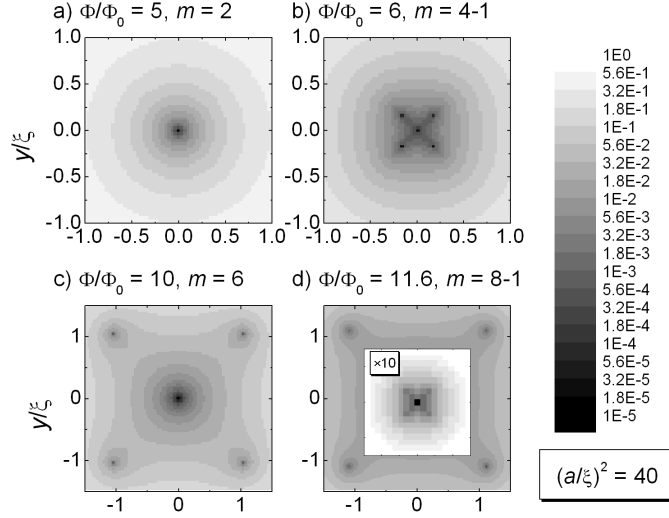


Figure 1. The modulus of the order parameter $|\psi|$ at different magnetic fields. The parameter Φ is the total external magnetic flux through the sample. The inset in d) shows the central region in an expanded scale. Note the logarithmic intensity scale.

with included boundary conditions. Eq.(4) was therefore solved by the direct minimization of the corresponding functional using the conjugate-gradient method. Both techniques gave identical results.

2. Results

We investigate first the phase diagram in the regions where the solution with one antivortex and four vortices and one antivortex and eight vortices has been reported. In Fig.1 we present the change of a spatial pattern of the modulus of the order parameter $|\psi|$ when the vorticity changes from $m = 2$ (Fig.1a) to $m = 4 - 1$ (Fig.1b) and from $m = 6$ (Fig.1c) to $m = 8 - 1$ (Fig.1d).

In the cases $m = 2$ and 6 (Fig.1a and Fig.1b) we observe a giant double vortex in the centre. In the cases with $m = 4l - 1$ with $l = 1, 2$ instead of the giant triple vortex the symmetry induced square pattern of four vortices with the antivortex in the middle forms. The results of the calculations show that the region of the phase diagram where the symmetry induced antivortex solution has the lowest energy is broader than expected from the solution of the linearized GLE. As it is shown in Fig. 2 for $\kappa_{eff} = \infty$ the antivortex phase is stable up to $(a/\xi)^2 \sim 55$, depending on Φ/Φ_0 . For a finite κ_{eff} this region shifts to the higher field as $(a/\xi)^2$ increases (see Fig.2). In the Fig.3 we presented the calculated value of the sample free energy as a function of external field for $(a/\xi)^2 = 35$ and for two values of $\kappa_{eff} = 1, \infty$. Topological

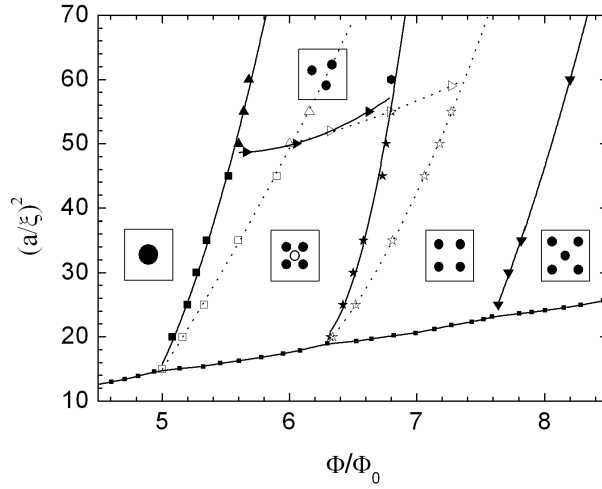


Figure 2. The calculated phase diagram. Different phases are marked with icons schematically indicating the vortex pattern where the full dot represents a vortex, the open dot represents an antivortex and the larger full dot represents a double vortex. The full symbols and continuous lines represent the phase boundaries for $\kappa_{eff} = \infty$ while the open symbols and dotted lines represent the phase boundaries for $\kappa_{eff} = 1$. In the later case only the phase boundaries of the region with the total vorticity 3 are shown.

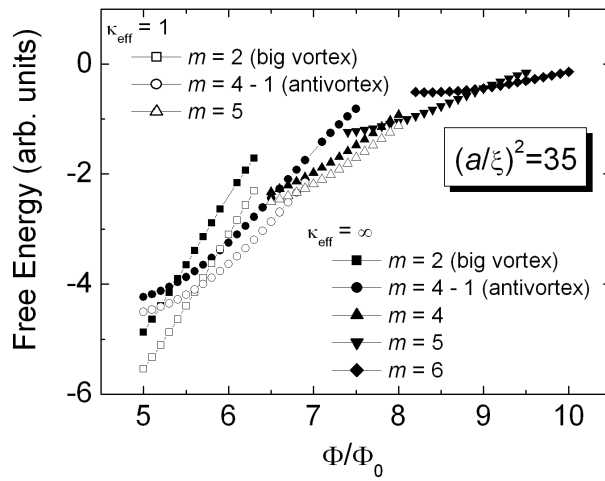


Figure 3. The free energy as a function of magnetic field for different vorticities m .

phase transitions with the changes of the total vorticity $\Delta m = 1$ are clearly seen. Reduction of κ_{eff} leads to the shift of the transition point to the higher field.

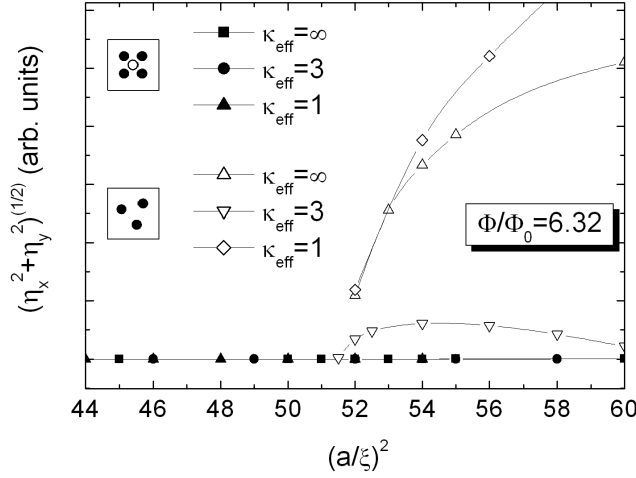


Figure 4. The magnitude of the order parameter around the transition where one vortex annihilates with the antivortex as a function of $(a/\xi)^2$ at the constant magnetic field.

The interesting behavior is observed when the external field is fixed and $(a/\xi)^2$ increases. Close to the H_{c2} the lowest minimum of the free energy corresponds to the solution with the vorticity $m = 4 - 1$ with the antivortex in the center of the square. Present calculations do not confirm the existence of the giant-vortex solution with $m = 3$ in this region of the phase diagram as reported previously [4]. The difference is due to increase of the number of discrete points N enabling detection of the antivortex. With increase of $(a/\xi)^2$ away from the H_{c2} line the phase transition to the multivortex state with the same vorticity ($m = 3$) and a lower symmetry takes place (see Fig. 2). In general, the free energy depends on the vorticity $m = n_+ - n_-$ and the total number of vortices in the system $n = n_+ + n_-$. The transition at $(a/\xi)^2 \sim 55$ and $\Phi/\Phi_0 \sim 5.5$ takes place at the constant vorticity $m = 3$ with the change of n from 5 to 3. The transition is therefore not only characterized by an order parameter, but also by the change of the number of vortices at the constant total vorticity m , suggesting that the transition is close to the first order. This statement is confirmed by the observation that above the transition point, $(a/\xi) > (a/\xi)_{crit}$, both solutions with $m = 3$ and $m = 4 - 1$ coexists. Since near the transition the free-energy difference between the phases with the same vorticity m and different n is small it is difficult to determine the phase boundary between phases with $m = 4 - 1$ and $m = 3$ accurately. The

transition could be easier observed by calculating the two component order parameter $\eta_x = \int x |\psi(x, y)|^2 dx dy$, $\eta_y = \int y |\psi(x, y)|^2 dx dy$ shown in Fig.4.

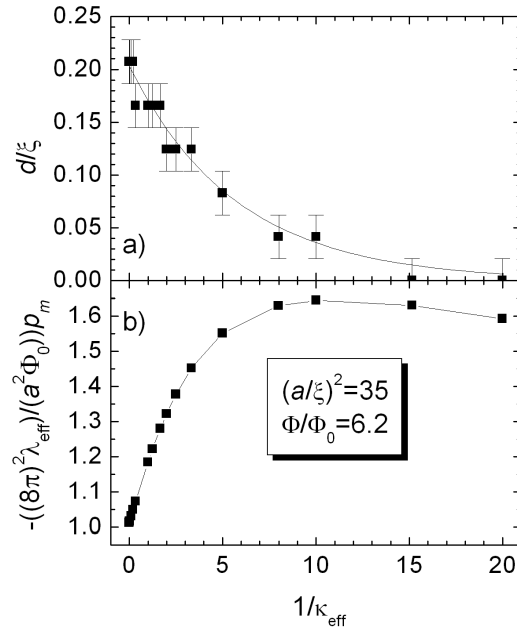


Figure 5. The vortex-antivortex distance a) and the magnetic moment of the sample b) as functions of the parameter $1/\kappa_{\text{eff}}$. In (a) error bars represent the grid spacing and the solid line the exponential fit discussed in the text.

Close to the H_{c2} line the repulsion of vortices from the boundaries and attraction of the 4 vortices to the antivortex stabilizes the phase with $m = 4 - 1$ and small vortex-vortex distances. At smaller value of ξ the repulsion from the boundaries decreases and one vortex annihilates with the antivortex. As a result, the repulsion between the remaining vortices increases leading to an increase of the order parameter with a further decrease of ξ .

Increasing the external field up to $\Phi/\Phi_0 = 11.6$ leads to the stabilization of the phase with total vorticity $m = 7$. Near the H_{c2} line similar to the case with $m = 4 - 1$ the solution with $m = 8 - 1$ is realized (Fig.1d). When $(a/\xi)^2$ increases in a complete analogy to the case with $m = 4 - 1$ the phase transition to the phase with $m = 7$ and a similar order parameter takes place. Here also, both solutions with $m = 8 - 1$ and $m = 7$ coexists above $(a/\xi)_{\text{crit}}$ indicating

that the transition is close to the first order. We believe that the situation is quite general for the case of arbitrary $m = 4l - 1$ for $l = 1, 2, 3, \dots$

At the end we would like to discuss the dependence of the stability of the antivortex phase at small κ_{eff} . According to the arguments of Ref.[8], at small κ the vortex-vortex interaction changes the sign making the antivortex phase more stable. As a result, the average distance between vortices in the middle of the square increases as well. In order to verify this conjecture for the thin film sample we plot in Fig.5 the vortex-antivortex distance r_0 as a function of $1/\kappa_{eff}$. The distance decreases with the decreasing κ_{eff} . For $\kappa_{eff} < 0.1$ the distance is smaller than the grid spacing a/N so we can not resolve separate vortices. We find that $r_0 \propto \exp(-\Lambda/\lambda_{eff})$ with $\Lambda \sim a$. The situation is just opposite to that reported in ref.[8]. We believe that in the case of the thin film of the square shape the reduction of κ does not stabilize the phase with the antivortex.

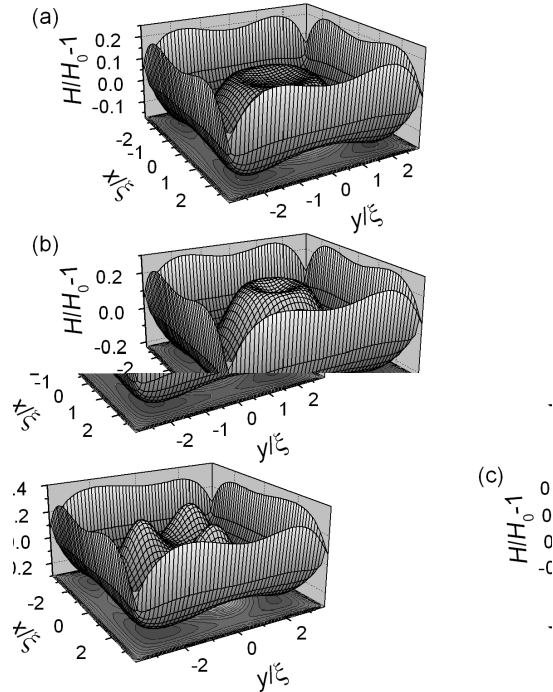


Figure 6. The magnetic field in the film in the case of (a) giant vortex with $m = 2$, (b) the antivortex solution with $m = 4 - 1$ and (c) three separate vortices with $m = 3$. Here H_0 is the external magnetic field.

It is interesting to note differences between samples of different shapes. For the cylindrical shape the giant vortex phase with any vorticity is always stable close to the H_{c2} line [10, 11]. According to Ref. [8] for the mesoscopic triangle the giant vortex state with $m = 2$ is metastable and the solution with the antivortex ($m = 3 - 1$) is stable. For the case of the square shape the giant vortex solution with $m = 3$ is *never* stable for $\kappa_{eff} \geq 0.1$. For $\kappa_{eff} < 0.1$ the limited grid spatial resolution prevented us to distinguish the solution with the antivortex from the possibly (meta)stable giant-vortex solution.

Finally, let us discuss the possibility to detect the state with the antivortex experimentally. Calculation of the magnetic field in the sample shows that the magnetic field has a local minimum in the center of the sample also for the giant vortex solution with $m = 2$. The local minimum observed for the antivortex state with $m = 4 - 1$ is therefore not due to the antivortex formation (Fig. 6) but due to a particular distribution of the current in the sample. Therefore, imaging of the magnetic field distribution cannot provide an evidence for the antivortex. The magnetic field for the multivortex solution with $m = 3$ has 3 well separated maxima that break the four fold rotational symmetry of the sample allowing a direct imaging of vortices. Since the antivortex state cannot be detected directly the observation of a hysteresis in the vicinity of the transition line from the $m = 4 - 1$ antivortex state to the $m = 3$ multivortex state could suggest that the symmetric phase is indeed the phase with the antivortex.

Acknowledgments

The authors wish to thank J. Bonca, A.S. Alexandrov and V.V. Moshchalkov for useful correspondence and discussions.

References

- [1] Chibotaru L.F., Ceulemans A., Bruyndoncx V., Moshchalkov V.V., Nature **408**, 833 (2000).
- [2] Abrikosov A.A., ZhETF, **32**, 1442 (1957).
- [3] Chibotaru L.F., Ceulemans A., Bruyndoncx V., Moshchalkov V.V., Phys. Rev. Lett. **86**, 1323 (2001).
- [4] Bonca J., V.V. Kabanov V.V., Phys. Rev. **B65**, 012509, (2002).
- [5] Baelus B.J., Peeters F.M., Phys. Rev. **B65**, 104515, (2002).
- [6] Melnikov A.S. et al, Phys. Rev. **B65**, 140503, (2002).
- [7] Mertelj T., Kabanov V.V. Phys. Rev. **B67**, 134527, (2003).
- [8] Misko V.R. et. al., cond-mat/0203140.
- [9] de Gennes P.G., 'Superconductivity of Metals and Alloys', Preus Books Publishing L.L.C. 1989.
- [10] Schweigert V.A., Peeters F.M., Deo P.S., Phys. Rev. Lett. **81**, 2783 (1998).
- [11] Schweigert V.A., Peeters F.M., Phys. Rev. Lett. **83**, 2409 (1999).